# Direct Measurements of Critical Stresses and Cracking in Thin Films of Colloid Dispersions

Weining Man and William B. Russel

*Department of Chemical Engineering, Princeton University, Princeton, New Jersey 08544, USA*

(Received 3 November 2007; published 13 May 2008)

Useful films can be formed by drying colloidal dispersions, but the negative capillary pressure generated often promotes cracks. Complex lateral flows during drying compromised previous measurements of the pressure required for cracking. Here we report data for the onset of cracking, and the additional cracks that appear at higher pressures, from high-pressure ultrafiltration experiments on homogeneously compressed films. A comparison of the data with expectations from theory confirms that cracking is controlled by elastic recovery, though an energy criterion only provides a lower bound. Our experiments also identify the role of flaws as nucleation sites that initiate cracks.

DOI: 10.1103/PhysRevLett.100.198302 PACS numbers: 82.70.Dd, 83.80.Hj

Dispersions of colloidal particles in the form of polymer latices or inorganic oxides, e.g., silica or alumina, are often coated on substrates to make thin films for various applications, for example, protective or decorative architectural coatings, ink jet papers, magnetic tapes, photographic film, antireflective coatings on lenses, synthetic opals, photonic crystals, and encapsulated vitamins. During drying, polymer-liquid, air-liquid (capillary pressure), or polymer-air interfacial tension may deform the particles enough to form a void-free film [1,2]. However, at low temperatures for which viscous deformation does not keep up with evaporation or with inorganic particles that do not deform viscously, films of close-packed particles can develop cracks while still saturated with liquid. Cracking during drying has been studied in a variety of systems, including ceramic films [3], polymer latices [4,5], and latex-inorganic mixtures [6]. Often parallel cracks follow a drying front, propagating from the edge of the film toward the wetter central regions [3,4,6] with spacing proportional to the film thickness [7–9]. In uniform films, there exists a critical thickness below which cracking does not occur [3,4]. Clearly understanding the mechanism of cracking in terms of the driving forces and the roles of the various physical-chemical properties of the colloidal suspension is essential for avoiding cracking to improve applications and for controlling the patterns formed by fractures [7].

In this study, we measure directly the capillary pressure at which homogeneous films of different thickness, formed from latex or silica dispersions of different radii, crack. Within a high-pressure ultrafiltration cell (Fig. 1 left), the consolidation process is driven by air pressure, rather than nonuniform evaporation, and involves only fluid flow normal to the film without laterally propagating drying fronts. We interpret these measurements through predictions [10], based on recovery of elastic energy calculated from stress-strain relations accounting for Hertzian [11] contact mechanics for saturated films, for the capillary pressure necessary to open a single infinite crack and the crack spacing expected at higher pressures.

During drying, evaporation of solvent, assumed hereafter to be water, first concentrates the particles into a uniform close packing, provided evaporation is slow relative to diffusion of particles across the layer and interparticle attractions are not abnormally strong. Further evaporation then pulls menisci at the top layer of particles downward, generating a negative capillary pressure $p_{\mathrm{cap}} < 0$ in proportion to the surface tension of the liquid $\gamma$ and the curvature of the meniscus. This puts the particle network in compression normal to the surface and in tension in the plane of the film, since the substrate prevents deformation laterally [5]. If the water-air interface recedes into the film leaving empty pores between particles, lateral gradients in the capillary pressure can tear the film apart [12]. In this case, the critical pressure for cracking $p_{\mathrm{cap}}^{\mathrm{crit}}$ would equal the maximum capillary pressure, for example, $\sim -5.3\gamma/a$ in a dense packing [13], which is inversely proportional to particle radius $a$, and independent of film thickness $H$ and shear modulus $G$ of the particles. When the water-air interface remains at the surface and the film is constrained by the substrate, cracks can open when the elastic energy recovered exceeds the increase in surface energy [10].

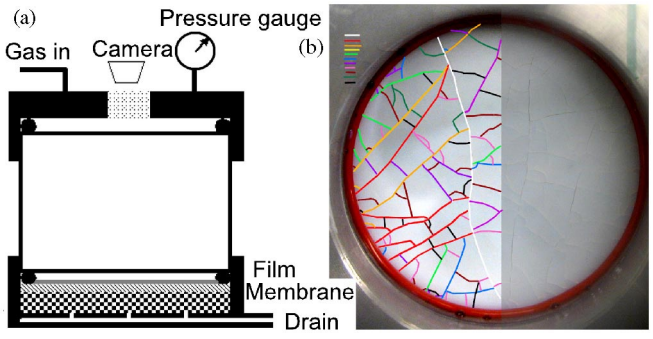


FIG. 1 (color online). (a) Schematic of pressure filtration cell with film (gray) confined by O ring ● and membrane in hatched area. (b) A cracked film with the first crack highlighted in white. Cracks on the left half are highlighted in different gray scales (color scale) corresponding to the increasing steps in pressure.

 

Hence, the critical capillary pressure $p_{\mathrm{cap}}^{\mathrm{crit}}$ should be independent of particle size and interparticle forces and depend only on the film thickness $H$, the shear modulus $G$ of the particles, and the surface tension $\gamma$. Dimensional analysis then specifies only two dimensionless groups and requires the dimensionless pressure $Hp_{\mathrm{cap}}^{\mathrm{crit}}/\gamma$ to depend only on the dimensionless modulus $GH/\gamma$. Therefore, identifying the cracking mechanism requires measurement of the corresponding capillary pressure as a function of film thickness, particle modulus, particle size, etc.

Indeed, experiments in the past have focused on the critical capillary pressure $p_{\mathrm{cap}}^{\mathrm{crit}}$ or the critical thickness $H_{\mathrm{cri}}$, below which films do not crack [3,4,6]. The tensile stress generated in a thin film during evaporation has been measured via the classical cantilever technique [4,5], which detects the deflection of the underlying elastic substrate. Unfortunately, drying on a narrow cantilever is rarely a one-dimensional process with spatially homogeneous stresses in the film. Instead, nonuniform evaporation generates water fluxes from the film center to the edge, which feed packing fronts that propagate inward as in directional drying from capillary cells open at one end [7]. The stresses across the film differ tremendously, causing the measured deflection, which reflects the average transverse stress in the film, to depend on the film dimensions and the exact location of the drying front. Even when the entire film reaches a saturated and close-packed state before cracking, the nonuniform thickness due to the lateral flow compromises the experiment. Singh and Tirumkudulu [14] took advantage of this nonuniformity to determine the critical thickness by spin-coating aqueous dispersions on glass substrates or silicon wafers and measuring the maximum thickness of crack-free regions in completely dried films.

In order to maintain a uniform film with no lateral flow or drying fronts while directly controlling the key variables, we fabricated a cylindrical high-pressure filter chamber sealed with Teflon O rings (Fig. 1 left). Thin films of colloid dispersions then were cast on an ultrafiltration membrane supported by a porous bronze disk. We employed polystyrene latices with glass transition temperatures well above ambient temperature with diameters (and polydispersity) of 696 nm (20%), 400 nm (20%), 155 nm (20%), and 91 nm (5%) and silica particles of 430 nm diameter and 10% polydispersity, as measured by dynamic light scattering. The shear modulus and Poisson ratio of polystyrene [15] are $1.19 \times 10^9$ Pa and 0.36, respectively, while those of silica are [16] $1.88 \times 10^{10}$ Pa and 0.25. High-pressure nitrogen gas introduced into the chamber slowly pushes the excess water in the dispersion through the membrane. Water vapor quickly saturates the air inside the chamber, suppressing further evaporation. A pressure (50 kPa) much lower than typical critical cracking pressure suffices to bring particles into close packing. Flow of water then stops and the film becomes more transparent. A higher applied pressure deforms the menisci between particles at the air-water interface, generating a negative capillary pressure that puts the dispersion in tension. This tension translates into an interparticle force of $O(a\gamma)$ that easily overcomes any interparticle repulsion of $O(kT/a)$, since $a^2\gamma/kT \sim 10^5$ for $a \sim 100$ nm and $\sim 10$ even for $a \sim 1$ nm. We then increase the pressure in small steps until the film cracks, to obtain a direct measure of the critical stress. Further increases in the pressure generate additional cracks that are recorded photographically after each step to determine the dependence of total crack number and average spacing on excess pressure. Figure 1 (right) provides a photograph of a cracked film with the first crack, and additional cracks corresponding to the increasing steps in pressure, highlighted. Similar cracking patterns were observed and modeled probabilistically in earlier literature [17]. These phenomena in open films drying from the top contrast with observations from directional drying of confined films open at one end, which often yield parallel cracks [7]. At the end, we quickly remove and weigh the film while wet and then after drying to determine the volume fraction and thickness. The initial volume factions varied from 0.10 to 0.40, while the final volume fractions after cracking were typically 0.61–0.65, i.e., near random close packing. The films are 64 mm in diameter and generally uniform and flat, though ultrathin films had somewhat thicker edges due to contact with the O ring.

Figure 2(a) presents the data for the capillary pressure $p_{\mathrm{cap}}^{\mathrm{crit}}$ at the onset of cracking as a function of film thickness, particle modulus, and particle size. For the 155 nm polystyrene sample, the critical pressure decreases with the thickness as $H^{-0.4}$ from 80 microns to 1100 microns. Furthermore, data for 155, 400, and 696 nm polystyrene latices fall in a single band, suggesting that the critical capillary pressure is independent of particle size. Data

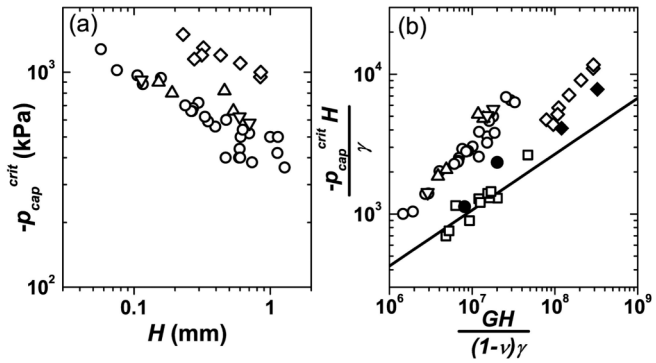


FIG. 2. (a) Capillary pressure at which first crack opened $p_{\mathrm{cap}}^{\mathrm{crit}}$ as a function of film thickness $H$ for dispersions of polystyrene latices of diameter 155 nm (○), 400 nm (△), and 696 nm (▽), and silica of 430 nm (◇). Note that $p_{\mathrm{cap}}^{\mathrm{crit}}$ is independent of particle size and increases with modulus. (b) Dimensionless critical capillary pressure plotted against dimensionless modulus for data from Fig. 1(a) along with additional experiments with scored O rings for polystyrene latices of diameter 155 nm (●), silica of 430 nm (◆), and polycrystalline 91 nm polystyrene latices (□) and the prediction from Eq. (1) (solid line).

from 430 nm silica particles show a similar power law dependence on film thickness, but are displaced to higher pressures as expected with the greater modulus of silica.

To better understand these trends, we turn to a recently published model [10] for the deformation of close-packed particles in response to capillary pressure at the free surface and tangential forces from the substrate. The theory is based on a relationship between stress and deformation or rate of deformation that reflects both the nature of the packing and the stresses within the particles, improving on both the classical Biot formulation [18] that assumes linear constitutive equations for elastic porous media and the *ad hoc* approximation of Routh and Russel [2] that derives a quadratic dependence of stress on strain. By exploiting the classical result of Hertz [11] relating force to deformation for elastic spheres and the generalization by Matthews [19] to viscous spheres, we have constructed a constitutive relationship for close-packed viscoelastic spheres in which the stress depends on the 3/2 power of the strain and rate of strain. Dispersion or van der Waals forces then are incorporated as contact adhesion due to particle-air or particle-water interfacial tension and rate of strain. Coupling these constitutive equations with the conservation of momentum allows us to address cracking via the energy criterion due to Griffith [20]. For this purpose we linearize about the uniaxially compressed base state and employ a thin layer approximation to calculate the relaxation of stress fields, both normal and parallel to the substrate, upon opening of a crack. The stress in the packing scales as $G\varepsilon^{3/2} \sim -p_{\mathrm{cap}}$, yielding a recovery of elastic energy upon opening a crack of $G\varepsilon^{5/2}H^2 \sim GH^2(p_{\mathrm{cap}}/G)^{5/3}$ per unit length. Balancing this against the surface energy expended, $\gamma H$, sets the scale for the capillary pressure necessary to open a crack as $G(\gamma/HG)^{3/5}$. Solution of the equations yields a quantitative lower bound on the capillary pressure necessary to open a single infinite crack, which increases with decreasing layer thickness as $H^{-3/5}$ and increasing shear modulus as $G^{2/5}$.

$$-Hp_{\mathrm{cap}}^{\mathrm{crack}}(\infty)/\gamma \cong 2.16[\phi NGH/2\pi(1-\nu)\gamma]^{2/5}, \quad (1)$$

where $N$ is the number of contacting neighbors, $\varphi$ is the volume fraction of the colloidal packing, and $\nu$ is the Poisson ratio, which conforms as it must with expectations from dimensional analysis as noted earlier. To open additional cracks, the capillary pressure must increase beyond that bound to recover sufficient elastic energy in less area. For parallel cracks with dimensionless spacing $w = W/2H$, we found that

$$p_{\mathrm{cap}}^{\mathrm{crack}}(\infty)/p_{\mathrm{cap}}^{\mathrm{crit}}(w) = \{\tanh(w) - w/[11\cosh^2(w)]\}^{3/5}. \quad (2)$$

Coupling the minimum capillary pressure for cracking with the maximum sustainable at the air-water interface ($-5.3\gamma_{wa}/a$) then yields the critical film thickness below which cracking will not occur, as $H_{\mathrm{crit}}/a = 0.049[\phi NGa/2\pi(1-\nu)\gamma]^{2/3}$.

Figure 2(b) compares the measurements with the prediction for $p_{\mathrm{cap}}^{\mathrm{crack}}(\infty)$ with $N = 6$ and $\varphi = 0.64$ (solid line). Clearly, the data from somewhat polydisperse polystyrene and silica particles do not fall on the same line, and both lie above our prediction. The latter suggests that the energy criterion for opening an infinite crack only provides a lower bound (necessary, but not sufficient) condition for crack formation, while the former indicates that other factors must be important. This motivated us to consider the role of flaws or defects in initiating cracks.

First, we tried highly monodisperse 91 nm polystyrene spheres with the expectation of achieving crystalline order and affecting the flaw distribution. As shown in Fig. 2(b), those data exhibit a similar power dependence on film thickness but at a lower critical pressure much closer to our prediction. The dynamics also differ significantly with the first crack in these films propagating slowly and tentatively across the film, unlike the initial cracks under higher pressures with the other particles, which raced quickly across the samples. The SEM images in Fig. 3 reveal a polycrystalline texture for the 91 nm monodisperse latices (left) that differs significantly from the random packing of the 155 nm polystyrene particles (middle), leading us to suspect that the grain boundaries act as large flaws to nuclei cracks close to the minimum capillary pressure. To confirm this hypothesis, we intentionally introduced flaws at the edge of the films by scoring the Teflon O ring constraining the colloidal film with a razor blade before the experiment. The results, shown as solid spheres and solid diamonds for 155 nm polystyrene and 430 nm silica, respectively, in Fig. 2(b), along with a photograph of the edge of those films as Fig. 3 (right), clearly demonstrate that flaws promote cracking at pressures closer to those predicted by our model.

To quantify the opening of additional cracks above the critical pressure $p_{\mathrm{cap}}^{\mathrm{crit}}$, we photographed the film at each step of increasing pressure. As discussed previously in Eq. (2), the energy criterion predicts the spacing between parallel cracks to decrease with increasing capillary pressure as the solid line shown in Fig. 4(a). The horizontal axis is the actual pressure $p_{\mathrm{cap}}$ normalized with the calculated

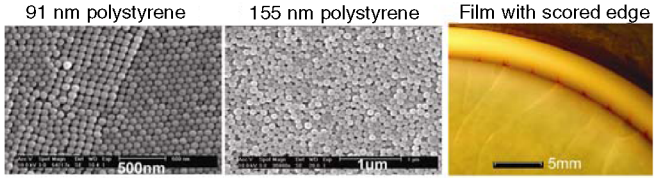


FIG. 3 (color online). Scanning electron microscope images of films after the experiments contrasting the polycrystalline order of the 91 nm polystyrene sample (left) with the disorder in the 155 nm polystyrene sample (middle). A photograph of the edge of a cracked film with cracks emanating from dark gashes in Teflon O ring (right).

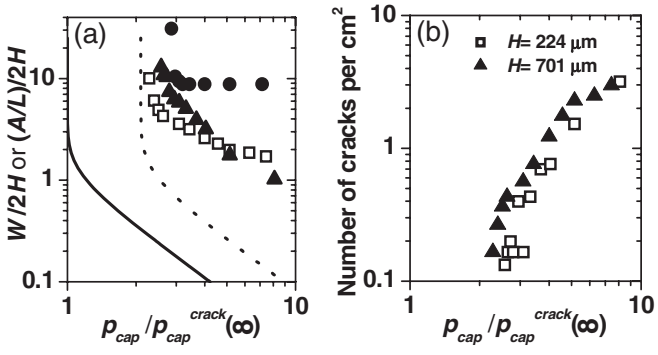


FIG. 4. Data for crack spacing and numbers as functions of the normalized capillary pressure $p_{\mathrm{cap}}$ relative to minimum. (a) Measured average crack spacing normalized on twice of the film thickness 224 $\mu$m (▲), 701 $\mu$m (□), and 935 $\mu$m (●) for 155 nm polystyrene and the predicted spacing between parallel cracks from Eq. (2) [solid line with $p_{\mathrm{cap}}$ normalized to theoretical $p_{\mathrm{cap}}^{\mathrm{crack}}(\infty)$; dotted line with $p_{\mathrm{cap}}$ normalized to average observed $p_{\mathrm{cap}} = 2.1 p_{\mathrm{cap}}^{\mathrm{crack}}(\infty)$]. Note that debonding (●) suppresses further cracking. (b) The number density of cracks at increasing normalized capillary pressure steps.

critical pressure $p_{\mathrm{cap}}^{\mathrm{crack}}(\infty)$, while the vertical axis is the crack spacing $W$ normalized with twice the film thickness $H$. Since the measured critical pressures are generally 2.1 times the calculated critical pressure $p_{\mathrm{cap}}^{\mathrm{crack}}(\infty)$, for comparison, the prediction normalized with $2.1 p_{\mathrm{cap}}^{\mathrm{crack}}(\infty)$ is plotted as the dotted line. The actual cracks are not parallel, but often nucleate at existing ones and propagate orthogonally, so we track the total length $L$ and number $N$ of cracks within the area $A$ of the film at each step and define $A/L$ as the average crack spacing and $N/A$ as the number density. The data in Fig. 4(a) for 155 nm polystyrene colloids show that the average spacing decreases with increasing stress, as expected, though much more slowly than predicted. When the film debonds from the substrate, cracking stops, independent of the extra pressure. Figure 4(b) presents the total number of cracks divided by the film area at increasing pressure $p_{\mathrm{cap}}$. Clearly the data do not follow the predictions for parallel cracks, suggesting that the available preexisting flaws or ones introduced by previous cracks limit the nucleation of additional cracks.

In this study, we achieved direct measurements of the pressure responsible for cracking in uniform films of latex or silica dispersions containing particles of varying radii by assembling a high-pressure filtration device. We find the critical capillary pressure to increase with decreasing film thickness and increasing particle shear modulus as predicted, but to consistently exceed the value predicted for a single infinite crack. Photographs taken at each pressure step yield the total length of cracks, which can be interpreted in terms of average crack spacing that decreases with increasing stress, as expected, though more slowly than predicted. Also, additional cracks often open at and propagate from existing ones, suggesting an important role of preexisting or newly created defects and flaws, as in linearly elastic materials. Intentionally introducing flaws at the edges or imparting polycrystalline order promotes cracking closer to the predicted critical pressure. Our experimental results confirm that the elastic energy recovery criterion provides a lower bound (a necessary, but not sufficient condition) for the capillary pressure at the onset of cracking, while demonstrating the importance of flaws to initiate cracks. These results improve our ability to anticipate the capillary pressure at which the first crack occurs and the thickness below which colloidal films do not crack.

This research was supported by the National Science Foundation through the Particulate and Multiphase Processes Program in the Division of Engineering Grant CTS No. 01-20421. We thank Paul M. Chaikin for his insistence that the critical pressure be measured directly and thank Ning Wu for discussions.

[1] P. R. Sperry *et al.*, Langmuir **10**, 2619 (1994).
[2] A. F. Routh and W. B. Russel, Langmuir **15**, 7762 (1999).
[3] R. C. Chiu and M. J. Cima, J. Am. Ceram. Soc. **76**, 2257 (1993); **76**, 2769 (1993).
[4] M. S. Tirumkululu and W. B. Russel, Langmuir **21**, 4938 (2005).
[5] M. S. Tirumkudulu and W. B. Russel, Langmuir **20**, 2947 (2004).
[6] C. Martinez and J. A. Lewis, Langmuir **18**, 4689 (2002).
[7] C. Allain and L. Limat, Phys. Rev. Lett. **74**, 2981 (1995).
[8] E. R. Dufresne *et al.*, Phys. Rev. Lett. **91**, 224501 (2003).
[9] W. P. Lee and A. F. Routh, Ind. Eng. Chem. Res. **45**, 6996 (2006).
[10] W. B. Russel, N. Wu, and W. Man, Langmuir 24, 1721 (2008).
[11] H. Hertz, J. Reine Angew. Math. **92**, 156 (1881).
[12] J. C. Brinker and G. W. Scherer, *Sol-Gel Science: The Physics and Chemistry of Sol-Gel Processing* (Academic Press, New York, 1990).
[13] G. Mason and D. W. Mellor, J. Colloid Interface Sci. **176**, 214 (1995).
[14] K. B. Singh and M. S. Tirumkudulu, Phys. Rev. Lett. **98**, 218302 (2007).
[15] G. Strobl, *Physics of Polymers* (Springer, New York, 1997), 2nd ed., p. 218.
[16] W. Kingery, *Introduction to Ceramics* (Wiley Interscience, New York, 1976), 2nd ed., p. 775.
[17] S. Bohn, L. Pauchard, and Y. Couder, Phys. Rev. E **71**, 046214 (2005).
[18] M. A. Biot, J. Appl. Phys. **26**, 182 (1955).
[19] J. R. Matthews, Acta Metall. **28**, 311 (1980).
[20] A. Griffith, Proc. R. Soc. A **221**, 163 (1920).